

This is the accepted version of the following article:

Xiaodong Ji\*, Mingliang Zhang, Hongzhen Kang, Jiaru Qian, Hongsong Hu. Effect of cumulative seismic damage to steel tube-reinforced concrete composite columns. *Earthquakes and Structures*, 2014, 7(2):179-200.

which has been published in final form at [[Link to final article](#)]

## Effect of cumulative seismic damage to steel tube-reinforced concrete composite columns

Xiaodong Ji<sup>1)</sup>, Mingliang Zhang<sup>2)</sup>, Hongzhen Kang<sup>3)</sup>, Jiaru Qian<sup>4)</sup>,  
Hongsong Hu<sup>5)</sup>

*1), 2), 4), 5) Key Laboratory of Civil Engineering Safety and Durability of China Education Ministry, Department of Civil Engineering, Tsinghua University, Beijing 100084, China*

*3) Department of Civil Engineering, Tangshan College, Tangshan 063000, China*

**Abstract.** The steel tube-reinforced concrete (ST-RC) composite column is a novel type of composite column, consisting of a steel tube embedded in reinforced concrete. The objective of this paper is to investigate the effect of cumulative damage on the seismic behavior of ST-RC columns through experimental testing. Six large-scale ST-RC column specimens were subjected to high axial forces and cyclic lateral loading. The specimens included two groups, where Group I had a higher amount of transverse reinforcement than Group II. The test results indicate that all specimens failed in a flexural mode, characterized by buckling and yielding of longitudinal rebars, failure of transverse rebars, compressive crushing of concrete, and steel tube buckling at the base of the columns. The number of loading cycles was found to have minimal effect on the strength capacity of the specimens. The number of loading cycles had limited effect on the deformation capacity for the Group I specimens, while an obvious effect on the deformation capacity for the Group II specimens was observed. The Group I specimen showed significantly larger deformation and energy dissipation capacities than the corresponding Group II specimen, for the case where the lateral cyclic loads were repeated ten cycles at each drift level. The ultimate displacement of the Group I specimen was 25% larger than that of the Group II counterpart, and the cumulative energy dissipated by the former was 2.8 times that of the latter. Based on the test results, recommendations are made for the amount of transverse reinforcement required in seismic design of ST-RC columns for ensuring adequate deformation capacity.

**Keywords:** steel-concrete composite column; cumulative damage; number of loading cycles; amount of transverse reinforcement; deformation capacity

### Nomenclature

$A_a$  = cross-sectional area of steel tube

$A_{ci}$  = cross-sectional area of infilled concrete

$A_{co}$  = cross-sectional area of RC encasement

$f_a$  = yield strength of steel tube

$f_c$  = axial compressive strength of concrete

$f_{ci}$  = axial compressive strength of infilled concrete

---

\* Corresponding author, Associate professor, E-mail: jixd@mail.tsinghua.edu.cn

$f_{co}$  = axial compressive strength of outer concrete

$f_{cu}$  = cubic compressive strength of concrete

$f_y$  = yield strength of steel

$f_{yv}$  = yield strength of transverse reinforcement

$H$  = height of LVDT 1<sup>#</sup> relative to column base

$N$  = axial load applied on column

$N_{ST-RC}^u$  = axial compressive strength of ST-RC column

$n$  = axial force ratio

$\Delta_u$  = ultimate displacement

$\Delta_y$  = yield displacement

$\eta$  = strength degradation factor

$\theta_y$  = yield drift ratio

$\theta_u$  = ultimate drift ratio

$\xi$  = confinement index of concrete-filled steel tube

$\rho_v$  = volumetric transverse reinforcement ratio

$\lambda$  = stirrup characteristic value (i.e., mechanical volumetric ratio)

### Subscripts

d = design value

t = test value

## 1. Introduction

With a judicious combination of steel and concrete, composite members possess the beneficial qualities of both materials. Two types of steel-concrete composite columns are frequently used in buildings constructed in earthquake-prone regions. One is the steel-reinforced concrete (SRC) column, and the other is the concrete-filled steel tube (CFST) column.

In the past decade, a new type of composite column, named the steel tube-reinforced concrete (ST-RC) column, has seen increasing use in China. The ST-RC column consists of a circular steel tube embedded in reinforced concrete. Fig. 1 shows the typical sections of ST-RC columns. The steel tube and its infilled concrete form the CFST core, and the outer concrete and reinforcing bars form the RC encasement. The CFST core located at the section center offers most of the axial compressive strength and shear strength, while the RC encasement located at the section periphery provides most of the flexural strength. High-strength concrete is often used for the CFST core to increase the compressive and shear strength of the column. Normal-strength concrete is used for the RC encasement for ensuring good ductility under cyclic bending. Such cross-sectional arrangement endows the ST-RC columns with remarkable advantages over the conventional composite columns, as presented in Ji et al 2014.

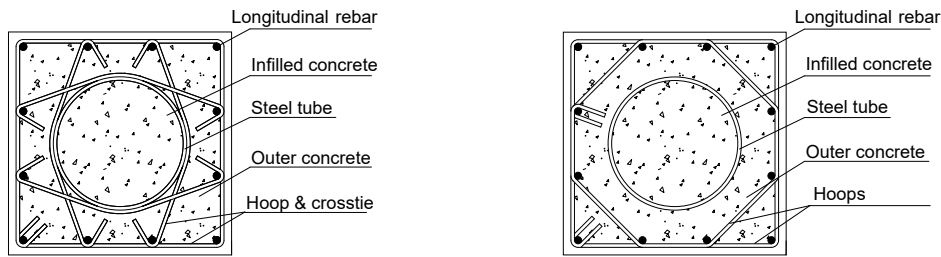


Fig. 1. Steel tube-reinforced concrete (ST-RC) composite column

Much effort has been devoted to studying the behavior and design of ST-RC columns (for example, Kang et al. 2006, Nie et al. 2008, Han et al. 2009, and Ji et al. 2014). The technical specification for ST-RC column structure CECS 188:2005 has been developed. Nevertheless, cumulative damage to ST-RC columns is an area yet to be studied comprehensively because of the short history of ST-RC columns. In all past quasi-static tests used to examine the seismic behavior of ST-RC columns, two or three cycles of the lateral loading were repeated at each drift level. These loading protocols may not fully stimulate cumulative damage.

The 2011 Tohoku earthquake was a reminder to us all that long-period, long-duration motion can induce cumulative damage in high-rise buildings. In this earthquake, hundreds of high-rise buildings in Tokyo metropolitan experienced large vibrations with a duration of several minutes due to resonance caused by the long-period motions (Takewaki et al. 2011). The E-Defense shaking table tests proved that high-rise buildings could sustain severe cumulative damage induced by many cycles of inelastic deformations when subjected to long-period, long-duration motions (Chung et al. 2010 and Ji et al. 2011). For the past three decades, extensive research has been carried out on cumulative damage in RC structures (for example, Kawashima and Koyama 1988, El-Bahy et al. 1999, Erberik and Sucuoglu 2004, and Pujol et al. 2006) and in the steel structures (for example, Krawinkler and Zohrei 1983, Fajfar 1992, and Jiao et al. 2011). Many efforts have also been made to study the seismic behavior and damage of concrete-filled steel tubes (for examples, Varma et al. 2002, Tort and Hajjar 2004, and Perea 2010). Since ST-RC columns are mainly used in high-rise buildings in regions of high seismicity, there is a clear need to investigate the effect of cumulative damage on ST-RC columns.

This paper presents a series of quasi-static tests performed on ST-RC columns subjected to high axial forces and lateral cyclic loading. The numbers of loading cycles and the amount of transverse reinforcement are taken as test variables. The objective of the study is to accumulate test data on the cumulative damage of ST-RC columns, which is useful for developing a damage model of the column, and to identify the transverse reinforcement requirement for ensuring adequate deformation capacity of the columns. The second section details the experimental program where six large-scale column specimens are tested. The third section summarizes the experimental results, including the failure mode and hysteresis behavior. The fourth section presents the strength, deformation and energy dissipation capacity, and the strength degradation of the column specimens.

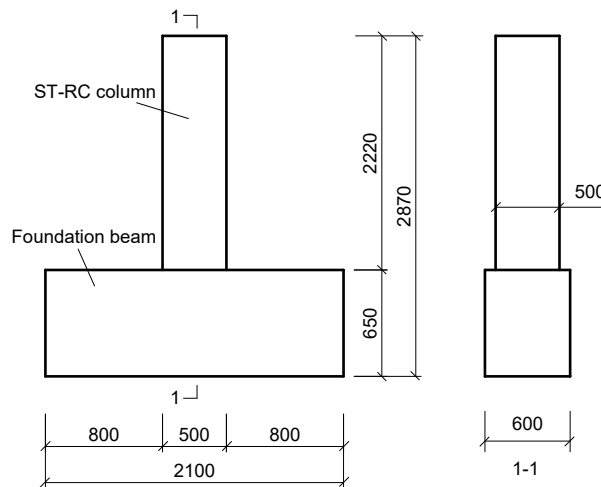
## 2. Experimental Program

## 2.1 Test Specimens

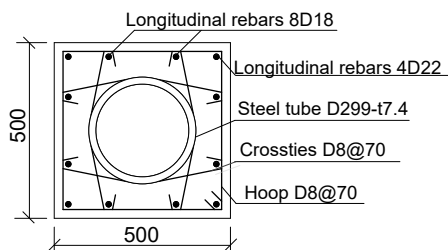
### 2.1.1 Specimen design

A total of six ST-RC column specimens labeled CC1 through CC6 were tested. The specimens were used to represent the frame columns in the lower story of a high-rise building and were fabricated at approximately half scale. Fig. 2 shows the geometries and reinforcement details of the specimens. The ST-RC column had a square cross section of 500 mm by 500 mm and a height of 2220 mm. The column was cast together with a RC foundation beam, with which the specimen was clamped to the rigid reaction floor.

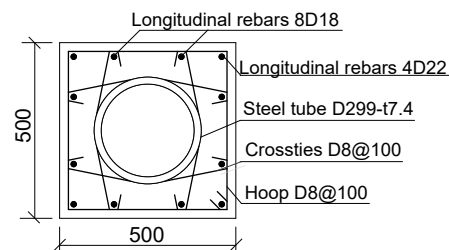
Four D22 (diameter = 22 mm) and eight D18 (diameter = 18 mm) steel rebars were used as the longitudinal reinforcement of the column, corresponding to an area ratio (i.e., the ratio of gross cross-sectional area of longitudinal rebars over that of the column) of approximately 1.4%. The transverse reinforcement consisted of perimeter hoops and bent crossties. D8 (diameter=8 mm) steel rebars were used as transverse reinforcement. Clear cover to hoops was 25 mm. The specimens were categorized into two groups according to the amount of transverse reinforcement. For Group I specimens (odd numbers in the nomenclature i.e., CC1, CC3, and CC5) the stirrups were distributed with a vertical spacing of 70 mm. Group II specimens (even numbers in the nomenclature i.e., CC2, CC4, and CC6) had a vertical stirrup spacing of 100 mm. The design for transverse reinforcement will be described in detail later. Note that all specimens were designed to satisfy the “strong shear and weak bending” mechanism, and that the tests results showed that the specimens failed in a flexural mode.



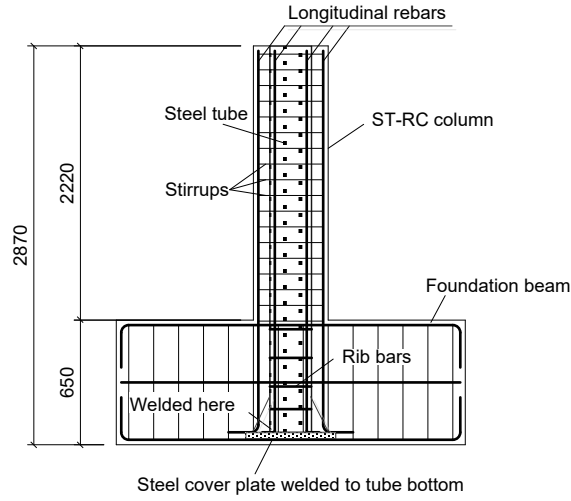
(a) Elevation view



(b) Section dimensions and reinforcement details for Group I specimens: CC1, CC3, CC5



(c) Section dimension and reinforcement details for Group II: CC2, CC4, CC6



(d) Elevation view of steel tube and reinforcement

Fig. 2 ST-RC column specimens (unit: mm)

A steel tube with outer diameter 299 mm, thickness 7.4 mm and diameter-to-thickness ratio 40 was embedded in the center of the column. A confinement index is used to quantify the extent of confinement of the infilled concrete by the steel tube (Han et al., 2004). The confinement index is defined as  $\xi = f_a A_a / (f_{ci} A_{ci})$ , where  $f_a$  denotes the yield strength of steel tube,  $f_{ci}$  denotes the axial compressive strength of infilled concrete, and  $A_a$  and  $A_{ci}$  denote the cross-sectional areas of the steel tube and infilled concrete, respectively. The CFST cores for all specimens had a confinement index of approximately 1.0. Note that the CFST core of the ST-RC column is commonly designed with a confinement index of around 1.0 in practical design. The ratio of the cross-sectional area of the CFST core to that of the column was 0.28 for all specimens.

Figure 2(d) shows an elevation view of the steel tube and rebars for the specimens. The steel tube and longitudinal rebars were securely anchored within the foundation beam with an anchorage depth of 600 mm. In addition, a thick steel end plate and four triangular stiffeners were welded at the base of the tube, and four rows of D12 rebars were welded along the tube perimeter as ribs, which further contributed to secure anchorage.

### 2.1.2 Material properties

Both the outer concrete and infilled concrete have design strength grade C45 (nominal cubic compressive strength,  $f_{cu} = 45$  MPa, and design value of axial compressive strength,  $f_{c,d} = 21.1$  MPa). Cubic compressive strength of the concrete was tested with cubes 150 mm in size, and five cubes were tested for each specimen. The average cubic strength of the concrete,  $f_{cu,t}$ , measured at the time of specimen testing are listed in Table 1. In accordance with the Chinese code for design of concrete structures (GB 50010-2010), the measured axial compressive strength of the concrete  $f_{c,t}$  was taken as 0.76 times  $f_{cu,t}$  for C45 grade concrete.

Both the longitudinal rebars and the transverse rebars are deformed steel bars. The D22 and D18 rebars have strength grade HRB400 (design value of yield strength,  $f_{y,d} = 360$  MPa). The D8 rebars have strength grade HRB335 ( $f_{y,d} = 300$  MPa). The tensile yield strengths of the D22, D18 and D8 rebars measured by coupon tests were 451, 470 and 372 MPa, respectively. The steel tube was fabricated from Q345 steel ( $f_{y,d} = 315$  MPa), and its yield

strength measured by coupon tests was 354 MPa.

Table 1 Parameters of specimens

Specimen No.	Concrete strength (MPa)		Confinement index	Axial force ratio		Volumetric transverse reinforcement ratio (%)		Stirrup characteristic value	
	$f_{cu,t}$	$f_{c,t}$	$\xi$	$n_d$	$n_t$	$\rho_{v,1}$	$\rho_{v,2}$	$\lambda_{d,1}$	$\lambda_{d,2}$
CC1	50.1	38.1	1.03	0.72	0.39	1.30	2.03	0.18	0.29
CC2	50.1	38.1	1.03	0.72	0.39	0.91	1.42	0.13	0.20
CC3	48.8	37.1	1.06	0.72	0.40	1.30	2.03	0.18	0.29
CC4	48.8	37.1	1.06	0.72	0.40	0.91	1.42	0.13	0.20
CC5	52.2	39.7	0.99	0.72	0.38	1.30	2.03	0.18	0.29
CC6	52.2	39.7	0.99	0.72	0.38	0.91	1.42	0.13	0.20

Note: 1) Subscripts d and t represent the design and test values, respectively;

2) Subscript 1 and 2 represent that the volumetric transverse reinforcement ratio are calculated by Methods 1 and 2, respectively.

### 2.1.3. Axial force ratio

The axial compressive force ratio (i.e., the normalised axial force in EuroCode 8) is one of the key parameters for the seismic design of a ductile column. An increase of the axial force ratio increases the depth of the compression zone of the column section and, therefore, decreases the ductility of the column. The axial force ratio of an ST-RC column is defined as follows (Ji et al. 2014):

$$n = \frac{N}{N_{ST-RC}^u} \quad (1)$$

$$N_{ST-RC}^u = f_{co} A_{co} + 0.9 f_{ci} A_{ci} (1 + \alpha \xi) \quad (2)$$

where  $n$  denotes the axial force ratio,  $N$  denotes the axial compressive load applied to the column,  $N_{ST-RC}^u$  denotes the axial compressive strength of the ST-RC column,  $f_{co}$  and  $A_{co}$  denote the axial compressive strength of the outer concrete and cross-sectional area of the RC encasement respectively,  $f_{ci}$  and  $A_{ci}$  denote the axial compressive strength and cross-sectional area of the infilled concrete respectively,  $\xi$  denotes the confinement index of the CFST core, and the coefficient  $\alpha$  is taken to be 2.0 if the cubic strength grade of the infilled concrete is less than C50, in accordance with Technical Specification JGJ 3-2011.

Evaluating Eqs. (1) and (2) with the design axial load and the design values of the material strengths gives the design value of the axial force ratio. While using the actual axial load and the measured material strengths in Eqs. (1) and (2) yields the test value of the axial force ratio. The load factor (i.e., the ratio of the design value of the axial load to the actual value) is given in the Chinese code for seismic design of buildings (GB 50011-2010) as 1.2. Allowing for both load factor and material strength reduction factor (i.e., the ratio of the

design value of material strength to the measured strength), the design value of the axial force ratio is approximately 1.9 times the corresponding test value.

The column specimens were subjected to a high axial force ratio to represent the columns at the base level of high-rise buildings. The axial compressive load was 5300 kN for all specimens. Table 1 shows the corresponding axial force ratio. The design axial force ratio  $n_d$  was 0.72 for all specimens, and the test value  $n_t$  varied slightly from 0.38 to 0.40.

#### 2.1.4 Design of transverse reinforcement

Transverse reinforcement is used to provide confinement to the concrete and to delay buckling of the compressed longitudinal rebars of the RC encasement. The amount of transverse reinforcement is expressed in terms of the stirrup characteristic value  $\lambda$  specified in GB 50011-2010 which is equivalent to the mechanical volumetric ratio specified in EuroCode 8. The stirrup characteristic value is calculated as  $\lambda = \rho_v f_{yv} / f_c$ , where  $f_{yv}$  and  $f_c$  denote the yield strength of transverse reinforcement and the axial compressive strength of the concrete respectively, and  $\rho_v$  denotes the volumetric transverse reinforcement ratio.

For design of ductile RC columns, both GB 50011-2010 and EuroCode 8 specify the lower limit of the amount of transverse reinforcement, which is related to the axial force ratios of the columns. The increase of the axial force ratio corresponds to an increased requirement for transverse reinforcement to ensure sufficient ductility of the RC columns. These well-established specifications for design of transverse reinforcement of RC columns are suitable for application to ST-RC columns.

A key issue is on the calculation method of the volumetric transverse reinforcement ratio for ST-RC columns. Fig. 3 shows the two methods to calculate the volume of the stirrup-confined concrete used for calculating the volumetric transverse reinforcement ratio. Method 1 uses the volume of all stirrup-confined concrete, including the CFST core (see Fig. 3(a)), while Method 2 uses the volume of only the stirrup-confined concrete of the RC encasement which excludes the CFST (see Fig. 3(b)). The CECS 188:2005 recommends Method 2. However, Method 2 would result in less transverse reinforcement than Method 1, given identical requirements for the volumetric transverse reinforcement ratio or the stirrup characteristic value.

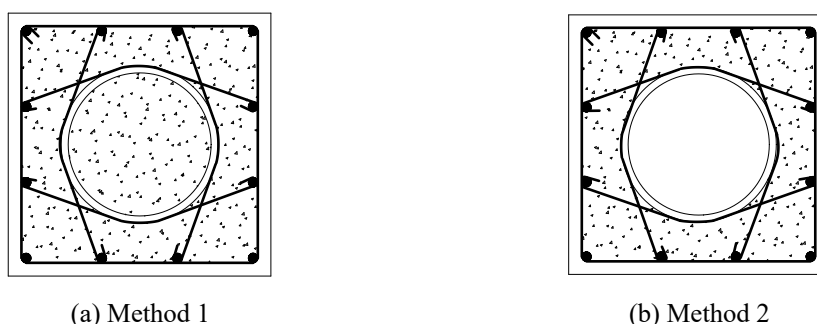


Fig. 3 Concrete area used for calculation of volumetric transverse reinforcement ratio

The ST-RC column specimens were designed to be seismic grade I columns (ductility columns) specified in GB 50011-2010. The required limit for stirrup characteristic value is 0.176 for columns under the design axial force ratio of 0.72. For comparison, the transverse reinforcement of Group I and II specimens were designed according to Methods 1 and 2, respectively. Table 1 shows the design stirrup characteristic values for the specimens. As

shown in Fig. 4, if using Method 1, the amount of transverse reinforcement of the Group I specimens satisfies the requirement for ductile columns, while the Group II specimens do not satisfy the requirement. However, if using Method 2, both groups of specimens satisfy the requirement.

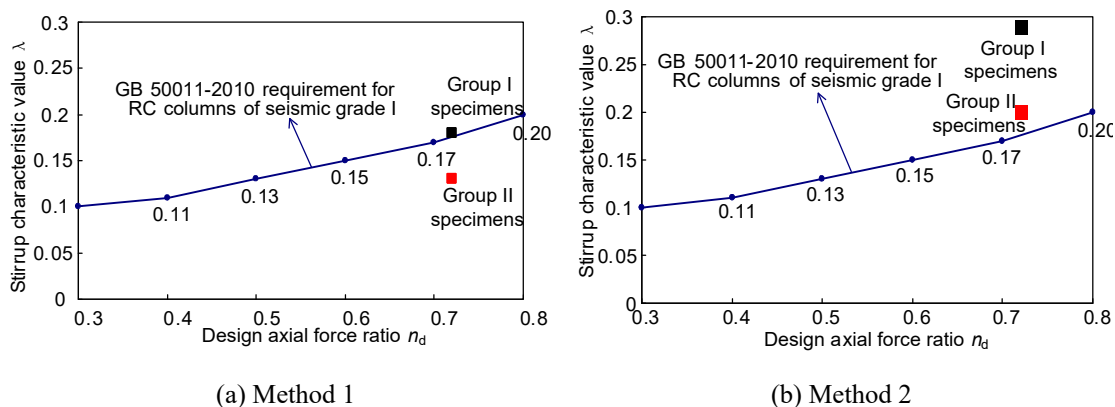
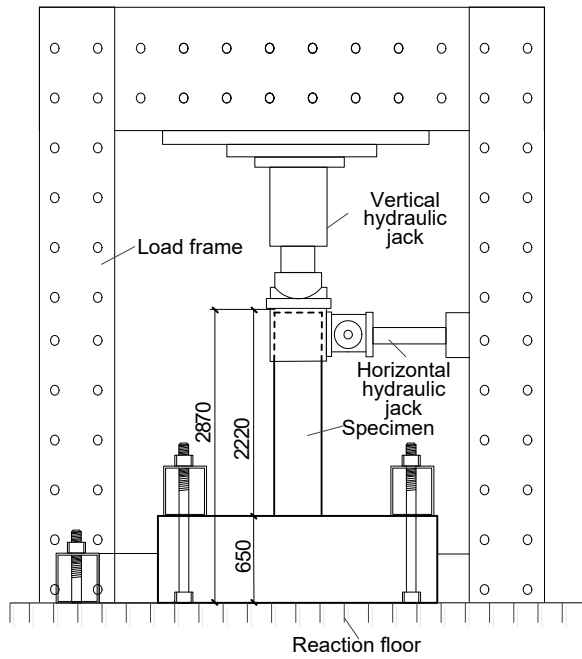


Fig. 4 Design axial force ratio versus stirrup characteristic value of specimens

## 2.2 Test setup and instrumentation

The test was conducted in the structural laboratory of Tsinghua University. The specimens were loaded by a large-scale multi-function loading device, which has a vertical loading capacity of 20 MN and a horizontal loading capacity of 3.5 MN. Fig. 5 shows the test setup. The foundation beam was securely clamped to the reaction floor. The top of the column was clamped to two hydraulic jacks, one in the horizontal direction and another in the vertical direction. The vertical jack could move freely in the horizontal direction to accommodate the lateral displacement of the specimens. Initially, a vertical load was applied to the specimen and was maintained at a constant value for the duration of the test. Afterwards, cyclic loads were applied quasi-statically by the horizontal hydraulic jack. The horizontal loading point was 2000 mm above the base of the column and thus the shear-to-span ratio of the specimen was 4.0.

Instrumentation was used to measure the loads, displacements and strains of the specimens. Load cells measured the vertical and lateral loads applied to the specimen. Fig. 6 shows the locations of the linear variable differential transformers (LVDTs) and strain gauges mounted on the specimen. Four LVDTs (LVDTs 1 through 4) measured the lateral displacements along the height of the column. Six LVDTs (LVDTs 5 through 10) were mounted at the base of the column to measure the local deformation from which the average vertical strains and the rotation in the plastic hinge region were estimated. Three LVDTs (LVDTs 11 through 13) were mounted on the foundation beam, one used to monitor the horizontal slip of the foundation beam along the reaction floor and the other two used to monitor the rotation of foundation beam during the loading. Strain gauges were installed to measure the strains of the longitudinal rebars and steel tube. The gauges were located 20 mm and 470 mm above the column base.

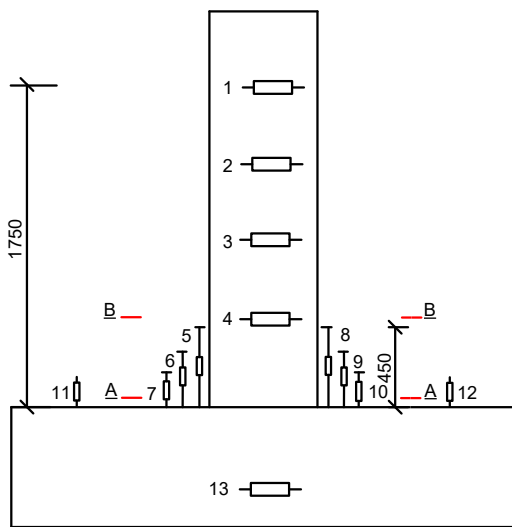


(a) Schematic of test setup

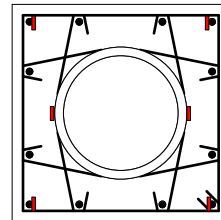


(b) Photo of test setup

Fig. 5 Test setup



(a) LVDTs



(b) Strain gauges at Sections A-A & B-B

Fig. 6 Specimen instrumentation

### 2.3 History of cyclic loading

The lateral loading was displacement-controlled, where the lateral displacement of the column top (monitored by LVDT 1 as shown in Fig. 6) was used for the control. Fig. 7 shows the history of lateral cyclic loading for the tests, which is similar to that used for cumulative damage tests on RC columns (Kawashima and Koyama 1988). The amplitudes

of lateral drift ratios increased in the sequence of 0.2, 0.35, 0.5, 0.75, 1, 1.5, 2, 2.5, 3, and 3.5%. Before the specimen yielded, one cycle of lateral loading was performed at each drift level. Afterwards, lateral loading was repeated multiple cycles at each drift level. Note that the yield drift of the specimen was slightly larger than 0.5%. In order to investigate the effect of cumulative damage, various numbers of cycles were considered. Three cycles were repeated for Specimens CC1 and CC2 at each drift level, five cycles for Specimens CC3 and CC4, and ten cycles for Specimens CC5 and CC6. In each loading cycle, a push was exerted first, followed by a pull, where a push is defined as positive loading and a pull as negative loading. The test was terminated when the specimen completely lost its lateral load-carrying capacity.

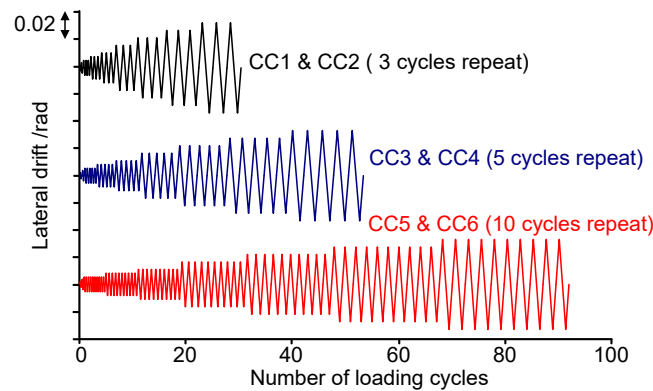


Fig. 7 Loading history

### 3. Experimental results

#### 3.1 Damage process and failure mode

The damage process of the ST-RC column specimens could be characterized by three stages: initial cracking stage, damage development stage and failure stage. The observations at each stage are summarized below.

**Initial cracking stage:** This stage spans from the onset of testing to the occurrence of the initial crack. When the lateral drift ratio reached 0.5%, horizontal flexural cracks initially appeared at the base of the column on tensile zone. The monitored strain data showed that the longitudinal rebars had yet to yield at the initial cracking drift.

**Damage development stage:** This stage is the period between the initial cracking and the peak load of the specimen being reached. Cracks at the base of the column gradually expanded and propagated toward the center of the column during this stage. More horizontal and inclined cracks were observed along the height of the column. The inclined cracks initiated from the tensile zone of the column during consecutive load reversals. At 0.75% drift, the longitudinal rebars in the compressive zone yielded. At 1.0% drift, slight vertical cracks caused by extremely large compressive strain developed at the corners of the column base, while the longitudinal rebars in the tensile zone and the steel tube did not yield at this drift. At approximately 1.5% drift, the specimen reached its peak lateral load. For all specimens, the longitudinal rebars in tension and the steel tube yielded at this drift. A flexure plastic hinge formed in the region from the column base up to a height equal to the column sectional depth. The concrete cover of Specimen CC6 spalled off, while the

concrete cover of the other specimens did not exhibit spalling at this stage.

**Failure stage:** This stage spans from the peak load to complete failure of the specimen. Table 2 shows failure process of the specimens. The concrete cover spalled off at 2% drift. As the drift was further increased, the longitudinal rebars buckled, and the transverse reinforcement failed, including pullout of the hooks of the crossties and hoop fractures. It is likely that the outward force of the buckling longitudinal bars against the hoops induced stress concentrations that contributed to hoop fractures. Finally, significant crushing of the outer concrete and local buckling of the steel tube occurred, which led to a loss of lateral load-carrying capacity of the column. Note that all specimens could carry the applied axial compressive load, which was mainly supported by the CFST core, even up until the end of the testing. This suggests the ST-RC column is well suited for preventing gravity load collapse during earthquakes.

Table 2 Failure process of specimens

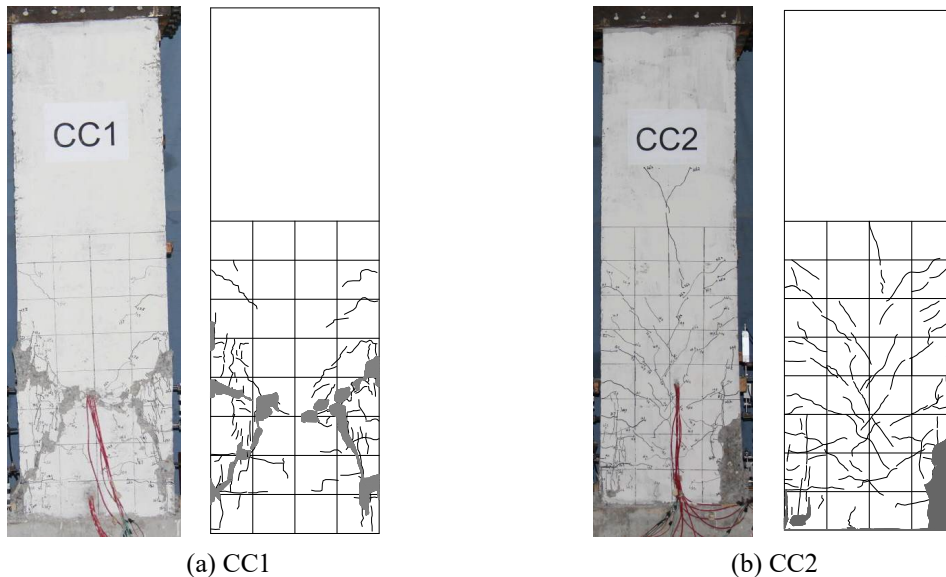
Specimen No.	2% drift	2.5% drift	3% drift	3.5% drift
CC1	Concrete cover spalled off.	Concrete cover spalled off.	Longitudinal rebars buckled.	Transverse rebars failed, outer concrete was crushed, and the steel tube buckled locally.
CC2	Concrete cover spalled off.	Concrete cover spalled off.	Longitudinal rebars buckled, transverse rebars failed, outer concrete was crushed, and the steel tube buckled locally.	Transverse rebars failed, outer concrete was crushed, and the steel tube buckled locally.
CC3	Concrete cover spalled off.	Concrete cover spalled off.	Longitudinal rebars buckled.	Transverse rebars failed, outer concrete was crushed, and the steel tube buckled locally.
CC4	Concrete cover spalled off.	Longitudinal rebars buckled, transverse rebars failed, outer concrete was crushed, and the steel tube buckled locally.		
CC5	Concrete cover spalled off.	Longitudinal rebars buckled.	Transverse rebars failed, outer concrete was crushed, and the steel tube buckled locally..	
CC6	Concrete cover spalled off, longitudinal rebars buckled, transverse			

rebars failed, outer  
concrete was  
crushed, and the  
steel tube buckled  
locally.

---

The data presented in Table 2 indicates that the drift ratio at complete failure of the specimen decreases with an increase in the number of loading cycles. For the Group I specimens, the drift at complete failure decreased from 3.5% to 3% when the number of loading cycles increased from 3 (Specimen CC1) to 10 (Specimen CC5). For the Group II specimens, the drift at complete failure decreased from 3% to 2% when the number of loading cycles increased from 3 (Specimen CC2) to 10 (Specimen CC6). It is also notable that the drift of the Group II specimen at complete failure was smaller than that of the Group I counterpart.

GB 50011-2010 specifies that the maximum drift limit for the RC frame structure subjected to the Maximum Considered Earthquake (MCE) is 2%. Fig. 8 shows photographs of the specimens after 2% drift loading. Specimens CC1 through CC5 experienced concrete cracking and slight spalling of the concrete cover, while Specimen CC6 had already reached complete failure at the level of drift. Note that major diagonal cracks formed in Specimen CC1, which is different from the cracking pattern of other specimens. The diagonal cracks are suspiciously similar to those caused by non-compactness of concrete, especially given the cracked region coincides with the location of the dense cables connecting to the strain gauges. At 2% drift, the post-peak strength decrease for Specimens CC1, CC2, CC3 and CC5 was less than 30%, and the strength decrease for Specimen CC4 was 35%. However, Specimen CC6 completely failed, with flexural strength close to zero.



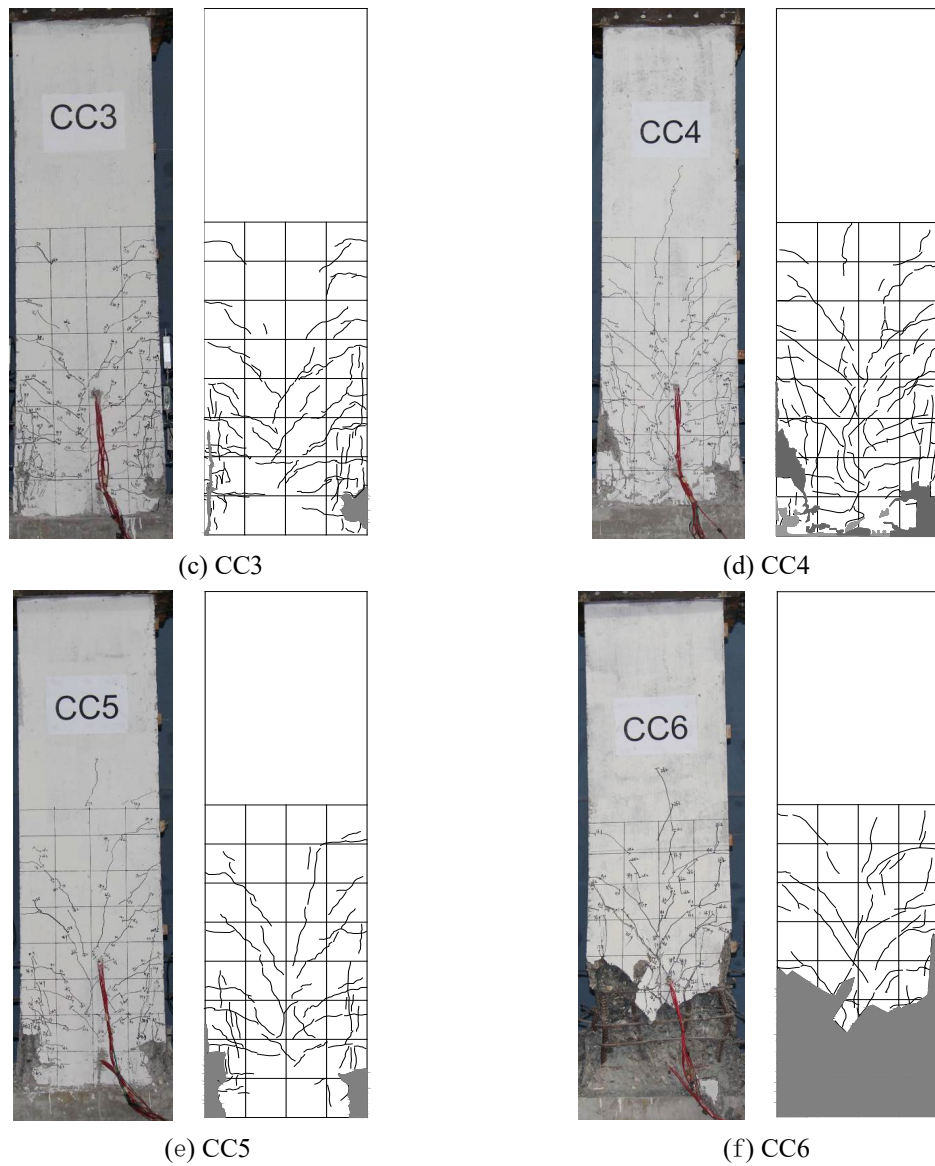
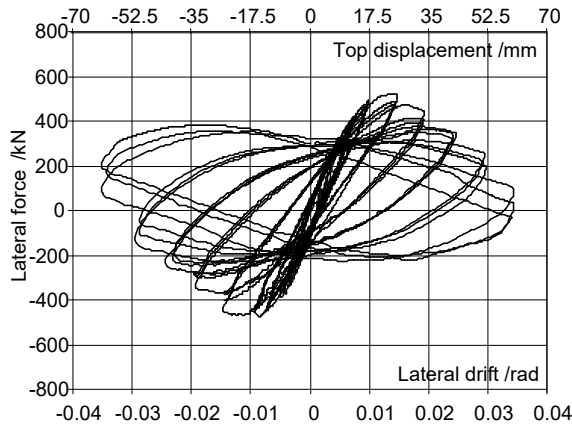


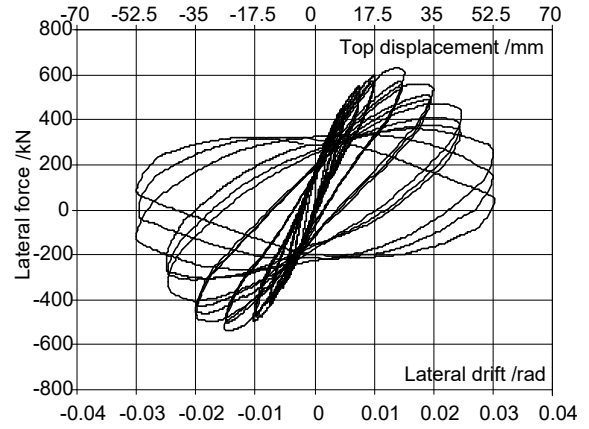
Fig. 8 Cracking patterns and photographs of specimens after 0.02 drift loading

### 3.2 Force-displacement relationship

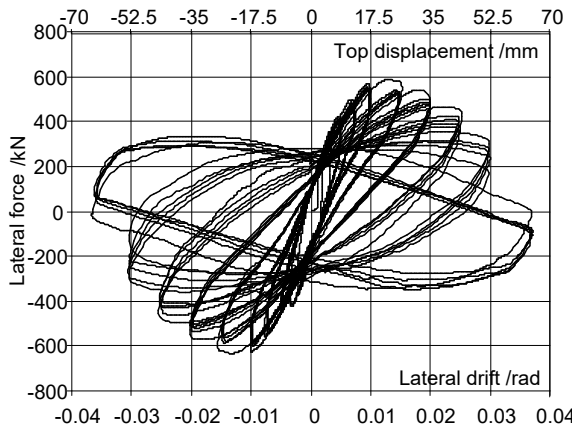
Fig. 9 shows the measured lateral force versus displacement relationship for all specimens. The hysteresis loops of all specimens were unpinched and full, demonstrating the inherent good energy dissipation characteristics for flexure failure of ST-RC columns. Since the  $P-\Delta$  effect was included, the hysteresis loops showed negative stiffness when the specimens approached complete failure. The hysteresis loops of the Group I specimens were wider than those of Group II. Before the specimen reached its peak load, the hysteresis loops of different cycles at the same drift loading were very close. After the peak load, the strength degradation of consecutive cycles at the same drift became very obvious.



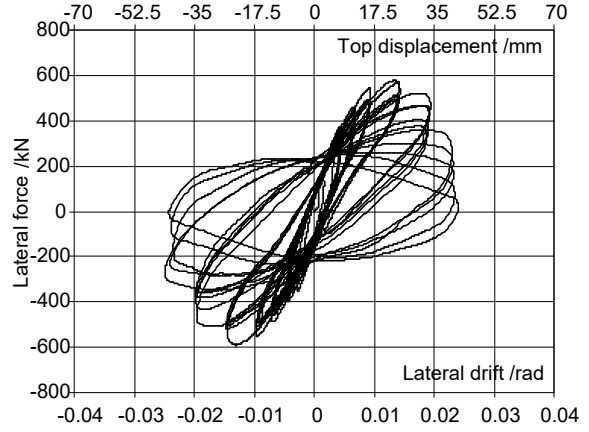
(a) CC1



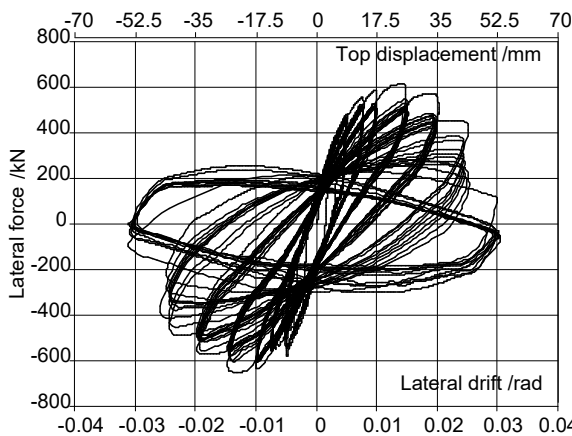
(b) CC2



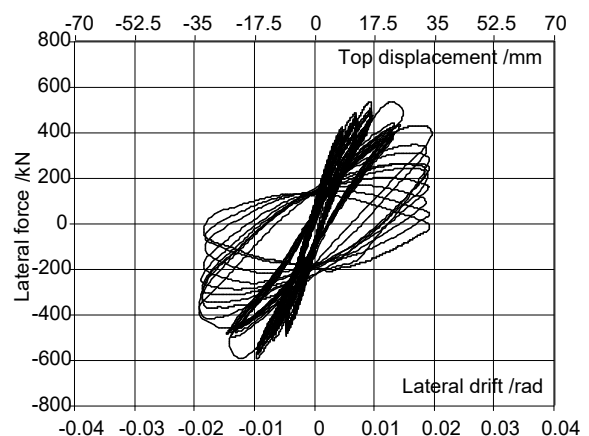
(c) CC3



(d) CC4



(e) CC5



(f) CC6

Fig. 9 Hysteretic loops of lateral force versus displacement relationships of specimens

#### 4. Strength, deformation and energy dissipation

##### 4.1 Strength capacity

Fig. 10 shows the peak lateral loads of the specimens. All Group II specimens had nearly identical peak loads, approximately equal to 580 kN. The Group I specimens, except for Specimen CC1, had peak lateral loads of around 620 kN. The numbers of loading cycles thus appears to have minimal effect on the strength capacity of the ST-RC columns. Note that the smaller peak load of Specimen CC1 was likely caused by the non-compactness of the concrete of Specimen CC1.

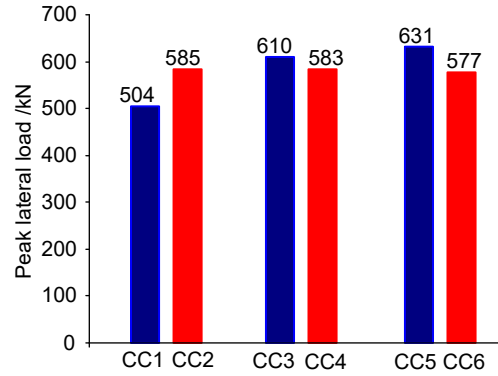


Fig. 10 Peak lateral load of specimens

The peak load of the Group I specimens (except for CC1) was on average 6% larger than that of the Group II specimens. The increased amount of transverse reinforcement made limited increase of the flexural strength of the ST-RC columns.

#### 4.2 Deformation capacity

Table 3 presents the yield displacement  $\Delta_y$  and ultimate displacement  $\Delta_u$  of the specimens. The yield displacement was determined using the concept of equal plastic energy so that the area enclosed by the idealized elastic-perfectly plastic envelope curve was the same as that of the measured envelope curve. The ultimate displacement  $\Delta_u$  was defined as the post-peak displacement at the instant when the lateral load decreased to 85% of the peak lateral load. The drift ratio was calculated as  $\theta = \Delta/H$ , where  $H$  is the height of LVDT 1 relative to the column base. Note that the values shown in Table 3 were calculated using the average values of the displacements measured in the push and pull directions.

Table 3 Deformation capacity of specimens

Specimens No.	Yield		Ultimate	
	Disp. $\Delta_y$ (mm)	Drift ratio $\theta_y$	Disp. $\Delta_u$ (mm)	Drift ratio $\theta_u$
CC1	11.25	0.64%	31.85	1.8%
CC2	12.85	0.73%	35.60	2.0%
CC3	10.00	0.57%	38.00	2.2%
CC4	11.30	0.65%	33.40	1.9%
CC5	9.00	0.51%	37.45	2.1%
CC6	9.85	0.56%	29.90	1.7%

#### 4.2.1 Effect of number of loading cycles

Fig. 11 shows the envelope curves of the lateral force versus drift relationship for the specimens, where the lateral force has been normalized with the peak load. All the specimens had nearly identical initial stiffness. Before the peak load, the envelope curves of Specimens CC3 and CC5 were almost identical, and those of CC2 and CC4 were similar. However, Specimen CC6 had a smaller drift at the peak load than Specimens CC2 and CC4. After reaching the peak load, the strength of the specimens decreased rapidly as the number of loading cycles increased. Table 3 indicates that the ultimate displacement of Specimen CC5 was 5% smaller than Specimen CC3. The effect of the number of loading cycles on the deformation capacity for the Group I specimens was not significant. However, for the Group II specimens, the ultimate displacement of Specimens CC4 and CC6 were 6% and 16% smaller than that of Specimen CC2. It is evident, therefore, that the number of loading cycles has an obvious influence on the deformation capacity of the Group II specimens.

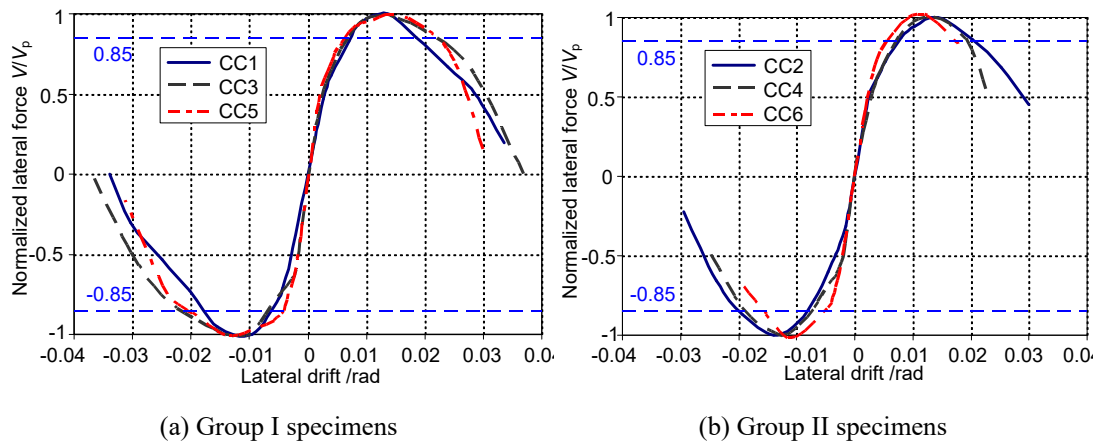


Fig. 11 Envelope curves of normalized lateral force versus drift ratio: Effect of number of loading cycles

#### 4.2.2 Effect of amount of transverse reinforcement

Fig. 12 compares the lateral force-drift envelope curves for specimens with varying amounts of transverse reinforcement. For Specimens CC3 and CC4 that were loaded five cycles at each drift level, the ascending branches of their envelope curves were almost identical. However, Specimen CC4, which had less transverse reinforcement, showed a more rapid strength decrease than CC3 after the peak load. Both Specimens CC5 and CC6 were loaded ten cycles at each drift level. Specimen CC6 had a smaller drift ratio at the peak load, relative to CC5, which had more transverse reinforcement, because the former sustained more severe cumulative damage. Similarly, Specimen CC6 showed a faster strength decrease than CC5.

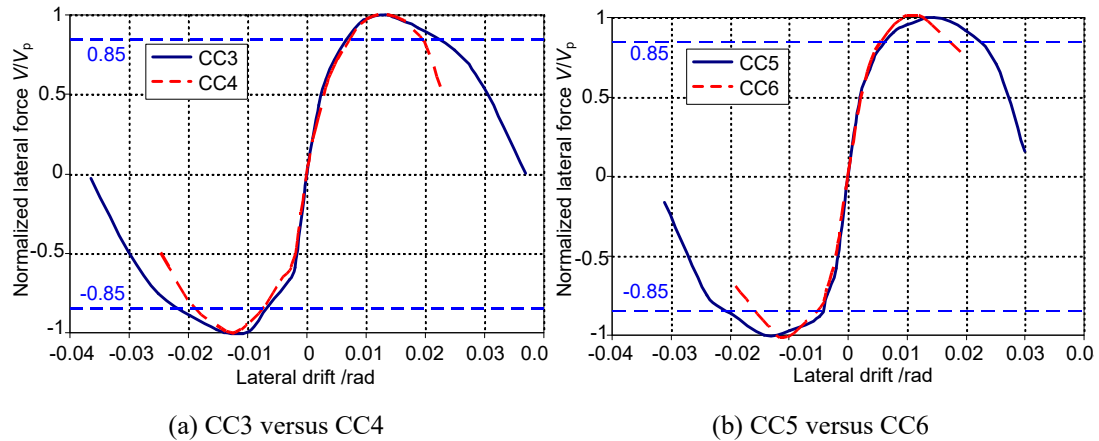


Fig.12 Envelope curves of normalized lateral force versus drift ratio: Effect of amount of transverse reinforcement

Table 3 indicates that the ultimate displacement of Specimen CC4 and CC6 were 13% and 25% smaller than those of CC3 and CC5, respectively. For the Group I specimens except for CC1, the ultimate drift was larger than 2% even when the lateral cyclic loads were repeated ten cycles at each drift. Note that the smaller ultimate drift of Specimen CC1 was suspiciously caused by the non-compactness of the concrete. For the Group II specimens, the ultimate drift reached 2% when the loading cycles repeated three cycles at each drift. However, when the number of loading cycles increased to five or ten, the ultimate drift was less than 2%.

Since the RC encasement is located at the section periphery, large plastic strains first develop in this region when the column is subjected to axial compression and bending moment. An increase of the confinement of the outer concrete can improve the hysteretic behavior of the RC encasement and, accordingly, improve the cumulative damage performance of the ST-RC column. Fig. 13 shows the hysteresis loops of the lateral force versus vertical strain of the outer concrete of Specimens CC5 and CC6. Note that the vertical strain was calculated by the measured vertical deformation of the column edge from the column base up to a height of 450 mm. Vertical plastic strain of the outer concrete for Specimen CC5 appeared to be stable during ten cycles of 2% drift loading. Owing to the reduced confinement provided by the transverse reinforcement, the compressive plastic strain for Specimen CC6 increased significantly during the loading cycles at 2% drift. This phenomenon correlated well with the test observation that the crushing of outer concrete was more rapid for the specimens that had less transverse reinforcement. Therefore, to ensure adequate deformation capacity for ST-RC columns subjected to cumulative damage, the outer concrete needs sufficient confinement. The transverse reinforcement of the ST-RC columns appears to require design based on the volume of all stirrup-confined concrete rather than just the volume of the RC encasement.

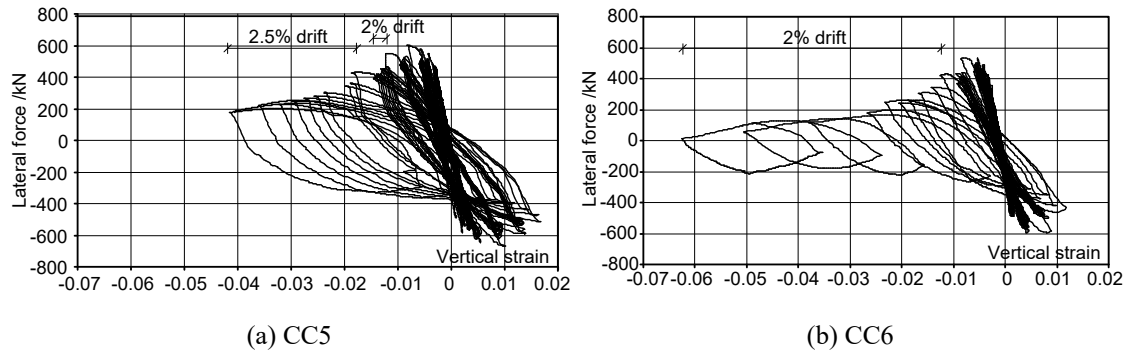


Fig. 13 Hysteresis loops of lateral force versus vertical strain for plastic hinge of specimens

### 4.3 Energy dissipation capacity

The energy dissipated in a loading cycle is given by the area surrounded by the corresponding hysteresis loop. Fig. 14 shows the average energy dissipated in a loading cycle for the specimen at varying drifts. The following observations can be made from this figure. (1) For Specimens CC3 and CC5, the average energy dissipated in a loading cycle at the same drift was almost equal. The average energy dissipated for Specimens CC2 and CC4 was almost identical, and was slightly larger than that of Specimen CC6. Therefore, the number of loading cycles had limited effect on the energy dissipated in a loading cycle, which is consistent with the past study for RC columns (Kawashima et al. 1988). (2) At 2% drift, the average energy dissipated by Specimens CC3 and CC4 was almost identical, and the average energy dissipated by Specimen CC5 was 13% larger than that of Specimen CC6. The amount of transverse reinforcement appears to have limited effect on the average energy dissipation. (3) Specimen CC1 had lower average energy dissipation in a loading cycle than other specimens, because of its lower strength.

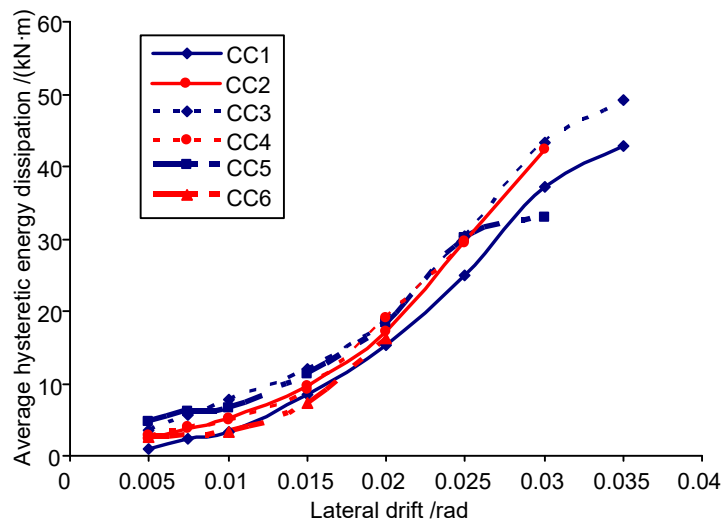


Fig. 14 Curves of average hysteretic energy dissipation versus drift ratio

Fig. 15 shows the cumulative energy dissipated by the specimens. The cumulative

energy dissipation is defined as the sum of the energy dissipated by the stable hysteresis loops before the lateral load decreases to 50% of the peak lateral load. Fig. 16 indicates that the cumulative energy dissipated by the Group I specimens (except for CC1) was significantly larger than that of the Group II specimens. The cumulative energy dissipation for Specimens CC3 and CC5 was 3.0 and 2.8 times that of Specimens CC4 and CC6, respectively. This is attributed to the fact that the former had increased deformation capacity compared to the latter, though they dissipated a similar amount of energy in each loading cycle.

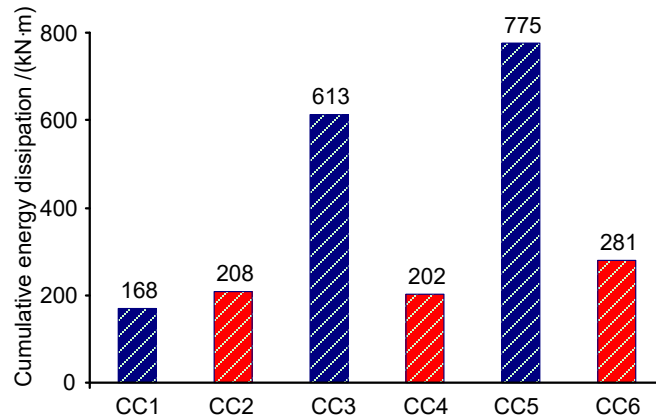


Fig. 15 Cumulative energy dissipated by specimens

#### 4.4 Strength degradation

The strength degradation factor for ST-RC columns is defined as the ratio of the maximum strength between the last cycle and the first cycle at the same drift level. Fig. 16 shows the strength degradation factor of the specimens. Before 1% drift, Specimens CC1 through CC6 had similar level of strength degradation. Afterwards, the flexural strength degradation was obviously related to the number of loading cycles. The increasing number of inelastic cycles could expedite the strength deterioration. In addition, the Group II specimens showed more rapid strength degradation than the Group I counterparts. At 0.02 drift, the strength degradation factor for the Group I Specimens remained over 0.8, while the factor for Specimen CC6 was close to zero.

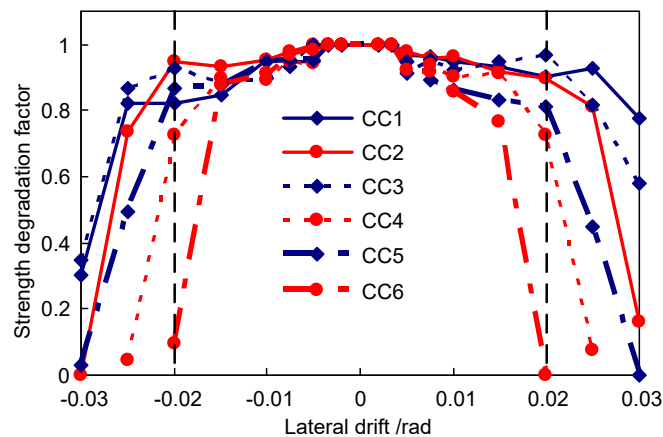


Fig. 16 Degradation of flexural strength of specimens

## 5. Conclusions

A series of quasi-static tests on large-scale ST-RC column specimens were conducted to examine the cumulative damage performance of ST-RC columns subjected to axial forces and lateral cyclic loading. Major findings obtained from the study are summarized as follows:

(1). The ST-RC column specimens showed a flexural failure mode, characterized by yield and buckling of longitudinal rebars, failure of transverse rebars, compressive crushing of concrete, and local buckling of the steel tube at the plastic hinge of the columns.

(2). The number of loading cycles made a small difference to the strength of the columns under combined axial force and bending moment.

(3). The number of loading cycles had limited effect on the deformation capacity of the ST-RC column specimens (Group I) for which the transverse reinforcement was designed based on the volume of all stirrup-confined concrete, while it had an obvious effect on the deformation capacity of the counterpart specimens (Group II) for which the transverse reinforcement was designed based on the volume of only the stirrup-confined concrete of the RC encasement.

(4). The Group I specimens showed larger deformation capacity than the corresponding Group II specimens. When the lateral cyclic loads were repeated five or ten cycles at each drift level, the ultimate drift of the former was 13% or 25% larger than that of the latter, respectively.

(5). The Group I specimens had significantly larger cumulative energy dissipation capacity than the Group II specimens. The cumulative energy dissipated by the former was around three times that of the latter.

(6). Increasing number of inelastic cycles significantly expedited the deterioration of flexural strength of ST-RC columns. The Group II specimens showed more rapid strength degradation than the Group I counterparts.

(7). Given that high-rise buildings might sustain severe cumulative damage when subjected to long-period ground motions, the recommendation is made that the transverse reinforcement for the ST-RC columns should be designed based on the volume of all stirrup-confined concrete.

## Acknowledgements

The work presented in this paper was sponsored by the National Natural Science Foundation of China (Grants No. 51261120377), Tsinghua University Initiative Scientific Research Program (Grants No. 2012THZ02-1 and No. 2011THZ03) and the National Key Technology R&D Program of China (2011BA09B01). The writers wish to express their sincere gratitude to the sponsors.

## References

CECS 188: 2005. "Technical specification for steel tube-reinforced concrete column structure." Beijing: China Planning Press, 2005 (in Chinese).

- Chung, Y., Nagae, T., Hitaka, T. and Nakashima, M. (2010). "Seismic resistance capacity of high-rise buildings subjected to long-period ground motions: E-Defense shaking table test." *Journal of Structural Engineering*, ASCE, **136** (6), 637-644.
- El-Bahy, A., Kunnath, S. K., Stone, W. C. and Taylor, A. W. (1999). "Cumulative seismic damage of circular bridge columns: Benchmark and low-cycle fatigue tests." *ACI Structural Journal*, **96**(4), 633-641.
- Erberik, A. and Sucuoglu, H. (2004). "Seismic energy dissipation in deteriorating systems through low-cycle fatigue." *Earthquake Engineering and Structural Dynamics*, **33**(1): 49-67.
- EuroCode 8. "Design Provisions for Earthquake Resistance-Part 1: General Rules, Seismic Actions and Rules for Buildings". Brussels: European Committee for Standardization, 2004.
- Fajfar, P. (1992) "Equivalent ductility factors, taking into account low-cycle fatigue." *Earthquake Engineering and Structural Dynamics*, **21**(10), 837-848.
- GB 50011-2010. "Code for seismic design of buildings." Beijing: China Ministry of Construction, 2010.
- GB 50010-2010. "Code for design of concrete structures." Beijing: China Ministry of Construction, 2010.
- Han, L. H., Yao, G. H. and Zhao, X. L. (2004). "Behavior and calculation on concrete-filled steel CHS (circular hollow section) beam-columns." *Steel & Composite Structures*, **4**(3), 169-188.
- Han, L. H., Liao, F. Y., Tao, Z. and Hong, Z. (2009). "Performance of concrete filled steel tube reinforced concrete columns subjected to cyclic bending." *Journal of Constructional Steel Research*, **65**(8-9), 1607-1616.
- JGJ 3-2011. "Technical specification for concrete structures of tall building". Beijing: China Ministry of Construction: Beijing, 2011 (in Chinese).
- Ji, X., Fenves, G. L., Kajiwara, K. and Nakashima, M. (2011). "Seismic damage detection of a full-scale shaking table test structure." *Journal of Structural Engineering*, ASCE, **137**(1), 14-21.
- Ji, X., Kang, H., Chen, X. and Qian, J. (2014). "Seismic behavior and strength capacity of steel tube-reinforced concrete composite columns." *Earthquake Engineering and Structural Dynamics*, **43**(4):487-505.
- Jiao Y., Yamada S., Kishiki S. and Shimada Y. (2011). "Evaluation of plastic energy dissipation capacity of steel beams suffering ductile fracture under various loading histories." *Earthquake Engineering and Structural Dynamics*, **40**(14), 1553-1570.
- Kang H. and Qian J. (2006). "Experimental study on high-strength concrete filled steel tube composite columns under axial compressive loading." *Proceedings of the Tenth East Asia – Pacific Conference on Structural Engineering and Construction*. Bangkok; 69-74.
- Kawashima, K. and Koyama, T. (1988). "Effect of number of loading cycles on dynamic characteristics of reinforced concrete bridge pier columns." *Structural Engineering/ Earthquake Engineering*, **5**(1), 183-191.
- Krawinkler, H. and Zohrei, M. (1983). "Cumulative damage in steel structures subjected to earthquake ground motions". *Computers and Structures*, **16**(1-4), 531-541.
- Nie J., Bai, Y. and Cai, C. S. (2008). "New connection system for confined concrete columns and beams. I: Experimental study." *Journal of Structural Engineering*, ASCE, **134**(12), 1787-1799.
- Perea T. (2010). "Analytical and experimental study on slender concrete-filled steel tube columns and beam-column." Ph.D. dissertation, School of Civil and Environmental Engineering, Georgia Institute of Technology, Atlanta, GA.
- Pujol, S., Sozen, M. A. and Ramirez, J. (2006). "Displacement history effects on drift capacity of reinforced concrete columns." *ACI Structural Journal*, **103**(2), 253-262.

- Takewaki, I., Murakami, S., Fujita, K., Yoshitomi, S. and Tsuji, M. (2011). "The 2011 off the Pacific coast of Tohoku earthquake and response of high-rise buildings under long-period ground motions." *Soil Dynamics and Earthquake Engineering*, **31**(11), 1511-1528.
- Tort, C. and Hajjar, J. F. (2004). "Damage assessment of rectangular concrete-filled steel tubes for performance-based design." *Earthquake Spectra*, **20**(4): 1317-1348.
- Varma, A. H., Ricles, J. M., Sause, R. and Lu, L. (2002). "Seismic behavior and modeling of high-strength composite concrete-filled steel tube (CFT) beam-columns." *Journal of Constructional Steel Research*, **58**(5-8): 725-758.